Infrared Spectroscopy of the Intramolecular Hydrogen Bond in Acethylacetone: A Computational Approach

I. Matanović and N. Došlić*

Department of Physical Chemistry, R. Bošković Institute, Bijenička 54, 10000 Zagreb, Croatia

Received: November 20, 2004; In Final Form: March 17, 2005

The intramolecular hydrogen bond in the *enol*-acethylacetone (ACAC) is investigated by performing reduced-dimensional quantum calculations. To analyze the shared proton vibrations, two sets of coordinates were employed: normal mode coordinates describing the motion in the vicinity of the most stable configuration, and internal coordinates accounting for the double minimum proton motion. It is proved that the extreme broadness of the OH-stretch band in ACAC is a consequence of the coexistence of two *enol*-ACAC structures: the global minimum and the transition state for rotation of the distal methyl group. Further, a ground-state tunneling splitting of 116 cm^{-1} is found, and it is shown that the inclusion of the kinematic coupling is mandatory when treating large-amplitude proton motion. In the OH-stretch direction a splitting of 853 cm^{-1} was predicted.

I. Introduction

For the past 20 years, the splitting of the ground vibrational level in malonaldehyde (MA) has been the subject of extensive experimental[1−3] and theoretical[4−8] study. Presently, as a result of significant methodological advances in both electronic structure and vibrational treatments,[9−12] the ground state tunneling splitting can be calculated with remarkable accuracy. Notwithstanding these successes, the understanding of splittings in the excited vibrational states, and of the vibrational spectra of intramolecular proton transfer (PT) systems in general, presents a significant challenge to theorists. Very recently three quantum mechanical studies considered the effects of the double-minimum potential on the O−H stretching vibration in MA. Consistently, a tunneling induced splitting of 152−158 cm^{-1} has been predicted. The assignments of the OH-stretch fundamental, however, differ largely. The six-dimensional approach of Hayashi and Mukamel[13] gave the ν_{OH} fundamental at 2491 cm^{-1}. The reaction path type calculation of Meyer et al.[10] on an approximate 21-dimensional PES yielded a frequency of 2282 cm^{-1}, while we obtained 2105 cm^{-1} using a three-dimensional Cartesian PES.[14] Unfortunately, spectroscopic information about the OH-stretching region in MA is scant, and, as long as linear-IR spectroscopy is concerned,[15] the very low intensity of the band prevents direct comparison between theory and experiment.[16]

The situation is rather different in acethylacetone (ACAC, Figure 1), a dimethyl derivate of MA about which a great deal of information is known.[17−24] The IR spectrum of ACAC is dominated by an extremely broadened OH-stretch band located between 1800 and 3400 cm^{-1} with a maximum at 2800 cm^{-1}.[17,21] It is widely recognized that such broadened band reflects strong mixing between the OH-stretch vibration and the low-frequency modes of the molecular scaffold.[25] Franck−Condon type vibrational progressions are expected to arise from combination transitions involving stretching of the hydrogen bond,[14,27] and the band-shape is further complicated by numerous Fermi-type resonances.[28,29] In principle, the double well motion of the bridging proton should also leave a mark in the OH-stretch region, but no unambiguous signature[31,30] of this kind has been found in the ACAC spectrum.

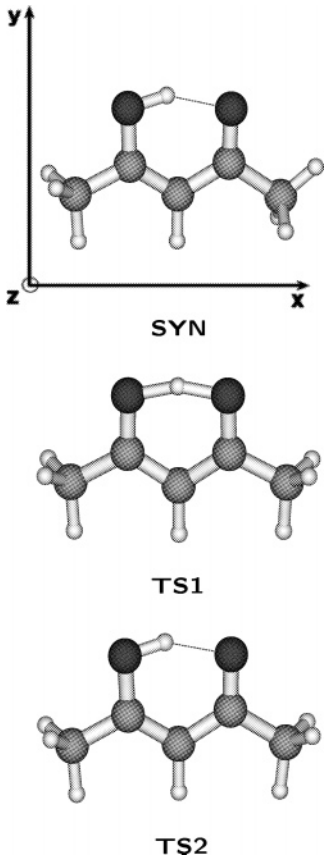

Figure 1. Relevant ACAC structures. From top to bottom: the global minimum structure (**SYN**), the transition state for the proton-transfer reaction (**TS1**), and the transition state for the rotation of the distal methyl group (**TS2**).

The present contribution is a detailed investigation of the vibrational spectrum of ACAC. More precisely, it is concerned with the part of the IR spectrum arising from the subset of modes

10.1021/jp044695s CCC: $30.25
Published on Web 04/19/2005

related to the H-bonding moiety. We simulated the vibrational spectrum assuming both small and large amplitude motion, i.e., on a single and on a double minimum potential energy surface, and are able to make a quantitative comparison between the two choices.

In ACAC the description of the H-transfer motion is complicated by its coupling to the internal rotation of the methyl groups (Figure 1). Although in the late eighties Horsewill and co-workers[32] established the presence of two energetically inequivalent methyl groups with hindering potentials of the order of 180 and 590 K (equivalent to 0.35 and 1.17 kcal mol^{-1}), direct evidence of the coupling is provided only recently by the inelastic neutron scattering experiment of Johnson et al.[19] Namely, in Johnson et al.[19] the frequency shifts of the methyl tunnel peaks upon deuteration of the enolic proton were observed.

To understand these coupling mechanisms we have investigated the reaction path connecting the C_{2v} transition structure, **TS1**, and the minimum energy configuration **SYN**.[33] It turned out that the methyl rotation and the PT reaction proceed in a non-synchronous manner; the PT reaction takes place only after the methyl groups have reached an eclipsed configuration **TS2**. This remarkable simplification allows us to treat the proton tunneling dynamics in ACAC using well-tested, localized, large-amplitude coordinates. Therefore, we will be able to provide an estimate of the ground state tunneling splitting in ACAC and investigate the impact of the double-minimum proton motion on the vibrationally excited states.

The paper is organized as follows. In section II we give the basic quantum chemistry information and outline the vibrational problem. In sections III and IV the numerical implementation of the single-well and double-well model is presented, and then the results are discussed. The paper is summarized in section V.

II. Electronic Structure Calculations

The stationary points relevant for the proton-transfer reaction in ACAC have been investigated by second and fourth-order Møller−Plesset perturbational theory (MP2, MP4), coupled cluster, and density functional theory (DFT). The DFT calculations were performed by using the B1LYP exchange-correlation functional.[34] All electron structure calculations were carried out with the Gaussian03 package.[35]

At all levels of theory the minimum energy structure of ACAC is confirmed to be the syn-enol isomer, **SYN**, with C_S point group symmetry shown in Figure 1.[24,33] The structures **TS1** and **TS2** are first-order saddle points and represent, respectively, transition structures for intramolecular proton transfer and for the rotation of the distal methyl group. The barriers for the rotation of the distal methyl group is estimated to be 0.26 kcal mol^{-1} at the MP2/6-311+G(d,p) level of theory, in agreement with the NMR spin−lattice relaxation time measurements.[32] At the same level of theory, a larger barrier of 1.45 kcal mol^{-1} is found for the rotation of the proximal methyl group.

The basis set dependence of the geometric and energetic properties of these stationary points was investigated in a previous work.[33] In Table 1 we confront the barriers for proton transfer and rotation of the distal methyl group at the MP2, MP4, and DFT/B1LYP levels of theory with reference coupled cluster results. The CCSD(T)/cc-pVTZ//MP2(FC)/cc-pVTZ barrier to proton transfer is 3.03 kcal mol^{-1} and the one for the rotation of the distal methyl group is 0.27 kcal mol^{-1}. Lower levels of theory predict proton-transfer barriers in the range between 2.15 (B3LYP/6-311+G(2d,2p)) and 3.41 (MP4/6-311+G(2d,2p)) kcal mol^{-1}. It is noteworthy that the barrier obtained at the moderate B1LYP/6-311G(d,p) level of theory is only 0.2 kcal mol^{-1} lower than the CCSD(T) result, and the remaining discrepancy is removed once we take into account that the PT reaction actually occurs in the **TS2** rotamer. In such case, a remarkably uniform value of 2.7 kcal mol^{-1} is obtained as an effective barrier to PT.

TABLE 1: Classical Energy Barriers for Proton Transfer (ΔE_1) and Rotation of the Distal Methyl Group (ΔE_2) Calculated on Various Levels of Theory

level of theory	ΔE_1/kcal mol^{-1}	ΔE_2/kcal mol^{-1}
B3LYP/6-311+G(2d,2p)	2.15	0.08
B1LYP/6-311G(d,p)	2.79	0.13
B1LYP/6-311+G(d,p)	2.79	0.09
B1LYP/6-311+G(2d,2p)	2.62	0.11
MP2(FC)/6-311G(d,p)	2.77	0.25
MP2(FC)/6-311+G(d,p)	2.64	0.26
MP2(FC)/6-311+G(2d,2p)	2.91	0.27
MP4(FC)/6-311+G(d,p)	3.01	0.24
MP4(FC)/6-311+G(2d,2p)	3.41	0.26
CCSD(T)/cc-pVTZ	3.03	0.27

Selected normal modes of ACAC in the **SYN** and **TS2** conformation are shown in Table 2. The geometries of these modes are strongly affected by the PT reaction, and one expects that the harmonic treatment will give a poor estimate of their vibrational frequencies. The size of the anharmonicity effect can be grasped from the difference between the harmonic and anharmonic frequencies,[36] but the disentanglement of the modes' coupling dynamics requires the computation of a multidimensional PES. The good agreement between the rather inexpensive B1LYP/6-311G(d,p) calculations and the much more sophisticated couple cluster approach made such an investigation possible.

II.1 Schrödinger Equation in Generalized Coordinates. For a set of M generalized coordinates, **q**, the vibrational kinetic energy operator is approximately given by[37]

$$\hat{T}_q = -\frac{\hbar^2}{2}\sum_{r=1}^{M}\sum_{s=1}^{M}\frac{\partial}{\partial q_r}\left[G^{rs}\frac{\partial}{\partial q_s}\right] \tag{1}$$

In the above equation G^{rs} is the element of the Wilson kinetic energy matrix and is equal to

$$G^{rs} = \sum_{i=1}^{3N}\frac{1}{m_i}\frac{\partial q_r}{\partial x_i}\frac{\partial q_s}{\partial x_i} \tag{2}$$

where N is the number of atoms involved in the vibrational problem, and $\{x_i\} \equiv x$ is the corresponding set of $3N$ Cartesian coordinates. In eq 1 the coordinate dependence of the Jacobian determinant $j = \det|\partial x_i/\partial q_j|$ is neglected, i.e., it is assumed that the determinant coordinate dependence is much smaller than that of the individual G^{rs} elements.[38]

The validity of further approximations depends on the type of coordinates used to formulate the vibrational problem. By neglecting the kinetic energy coupling term eq 1 simplifies to

$$\hat{T}_q \simeq -\frac{\hbar^2}{2}\sum_{r=1}^{M}\frac{\partial}{\partial q_r}\left[G^{rr}\frac{\partial}{\partial q_r}\right] \tag{3}$$

TABLE 2: Selected normal Mode Frequencies in cm^{-1} of the SYN and TS2 ACAC Conformers Calculated at the B1LYP/6-311G(d,p) Level[a]

			SYN		TS2	
mode	description	exp./gas	harm.	anharm.	harm.	anharm.
2	νOH	2800	3159	2766	3090	2487
9	ν_aC=C−C=O + δOH	1642	1700	1649	1690	1643
10	νC=O + δOH	1624	1659	1625	1655	1628
17	δOH + νC=O + C−C=C−O	1298[b]	1402	1345	1393	1318
18	δ_sCH$_3$ + δOH	1365	1394	1368	1401	1370
19	νC−C=C+ δOH + νC−CH$_3$	1250	1275	1242	1272	1242
34	νO···O	362	371	368	372	362
35	νOH···O	227[b]	230	238	234	224

[a] The IR gas phase data are taken from Tayyari et al.[21] [b] Raman/liquid.

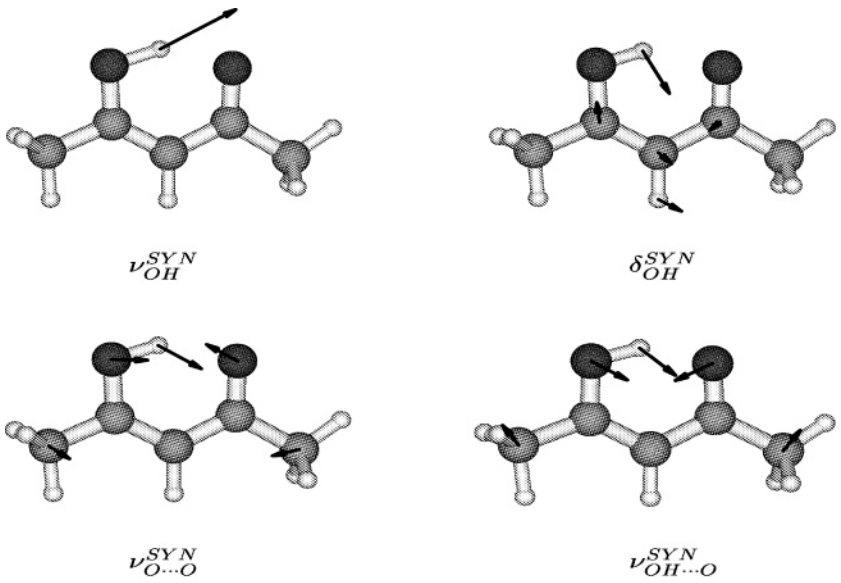

Figure 2. Normal mode displacement vectors of the **SYN** conformer. The four normal modes which span the 4D PES are: the OH-stretching ν_{OH}^{SYN}, the in-plane bending modes δ_{OH}^{SYN}, and two low-frequency skeleton modes $\nu_{O\cdots O}^{SYN}$ and $\nu_{OH\cdots O}^{SYN}$.

while the assumption of a constant G-matrix leads to

$$\hat{T}_q \simeq -\frac{\hbar^2}{2}\sum_{r=1}^{M}\sum_{s=1}^{M} G^{rs}\frac{\partial^2}{\partial q_s \partial q_r} \tag{4}$$

For orthogonal coordinates, such as normal modes, the kinetic energy operator acquires a simple form

$$\hat{T}_q = -\frac{\hbar^2}{2}\sum_{r=1}^{M}\left[G^{rr}\frac{\partial^2}{\partial q_r^2}\right] \tag{5}$$

In the following we will compare eqs 1−5 and identify those approximations that are most likely to introduce errors in the computation of ACAC eigenvalues.

III. Computational Aspects

III.1 Normal Mode Representation. The IR spectrum related to the OH···O fragment of ACAC is conveniently calculated using the normal mode representation of the Hamiltonian with the kinetic energy operator given by eq 5. In doing so we assumed that there is no total angular momentum and neglected the Coriolis coupling present in the full Watson Hamiltonian. The remarkable success of normal mode based approaches, such as the pairwise VSCF method[39−41] or fully coupled reduced dimensionality models,[14,42] in assigning vibrational spectra indicates that, under linear-IR conditions, the molecule samples only a limited region of the configuration space.

To span the coordinate space we have selected four normal modes of the ACAC's **SYN** conformer ($\{q_i^{SYN}\}$) and three normal modes of the **TS2** conformer ($\{q_i^{TS2}\}$). These modes, indexed with decreasing frequency, are the OH-stretching ν_{OH}^{SYN} (Table 2, ν_2), one of the in-plane bending modes δ_{OH}^{SYN} (ν_{17}), and two low-frequency skeleton modes, denoted as $\nu_{O\cdots O}^{SYN}$ (ν_{34}) and $\nu_{OH\cdots O}^{SYN}$ (ν_{35}). Figure 2 shows the atomic displacement vectors for the four **SYN** modes calculated at the B1LYP/6-311G(d,p) level of theory. For the **TS2** conformer we consider an analogous set of three normal modes: ν_{OH}^{TS2}, δ_{OH}^{TS2}, and $\nu_{O\cdots O}^{TS2}$. Due to the low barrier to the distal methyl group rotation, one expects an averaged ACAC structure at room temperature.

The potential energy and dipole moment surfaces were calculated at the same level of theory on a $q_1 \times q_2 \times q_3$ direct product grid with size 16 × 12 × 11. For **SYN** the range (Angstroms) was $-0.4 \le q_1^{SYN} \le 0.75$, $-0.7 \le q_2^{SYN} \le 0.7$, and $-1.6 \le q_3^{SYN} \le 1.6$. In the q_4^{SYN} direction 15 points were computed. Depending on the shape of the potential, a variable step size of 0.02 and 0.04 Å was used, resulting in a computation of 31680 symmetry unique points. The 3D grid for **TS2** was in the range (Angstroms) $-0.8 \le q_1^{TS2} \le 0.4$, $-0.6 \le q_2^{TS2} \le 0.6$, and $-1.5 \le q_1^{TS2} \le 1.3$.

Figure 3 presents six different two-dimensional cuts of the **SYN** and **TS2** PESs. In both conformers the OH-stretching coordinate mixes strongly with the low-frequency modes, and in **TS2** there is also a pronounced coupling with the bending coordinate.

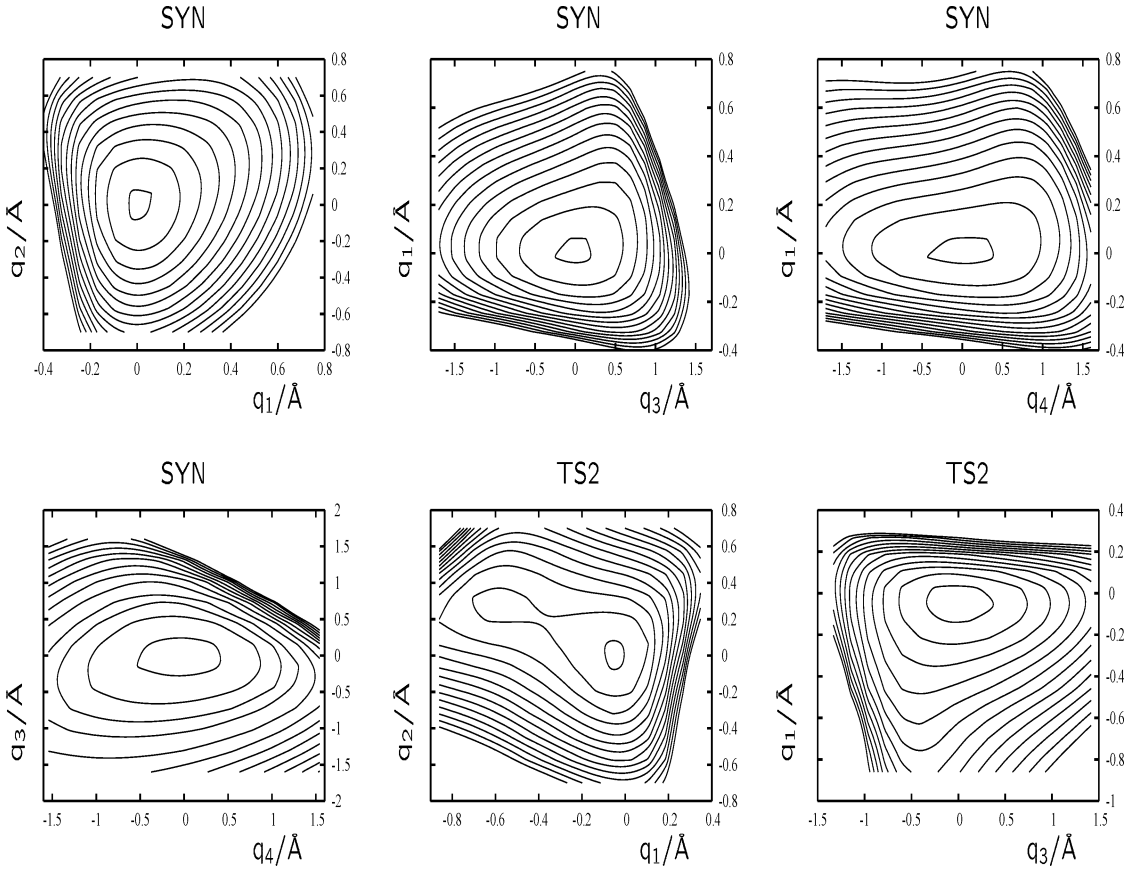

Figure 3. 2D projections of the potential energy surfaces (PESs) of **SYN** and **TS2**. The contours are drawn at each 0.4 eV, and the inner contour corresponds to an energy lying 0.1 eV above to the minimum of the PES.

The reduced mass μ_i for the *i*th vibrational mode is defined as[35]

$$\mu_i = (\sum_k^{3N} L^2_{\mathrm{CART}_{k,i}})^{-1}$$

where the column vectors of $L_{\mathrm{CART}_{k,i}}$ are the sets of coefficients with which the Cartesian displacements take part in a normal vibration, i.e., $\mu_i = N_i^2$ are the respective normalization factors. For the normal modes of interest, the following mass values in atomic mass units were obtained from ab initio calculations[35] at the minimum energy configuration. $\mu_{q1}^{\mathrm{SYN}} = 0.928$, $\mu_{q2}^{\mathrm{SYN}} = 0.540$, $\mu_{q3}^{\mathrm{SYN}} = 0.2473$, $\mu_{q4}^{\mathrm{SYN}} = 0.302$, and $\mu_{q1}^{\mathrm{TS2}} = 0.932$, $\mu_{q2}^{\mathrm{TS2}} = 0.417$, $\mu_{q3}^{\mathrm{TS2}} = 0.25$. The vibrational Schrödinger equation for the fully coupled potential, V(q1..q4), was solved using the Fourier grid Hamiltonian approach[43] on a 16-(32) × 16 × 16 × 16 grid combined with the implicitly restarted Lanczos diagonalization method[44] implemented in the ARPACK suites of programs.[45,46] In the 3D case the grid size was 32 × 32 × 32. The large number of computed points allowed us to circumvent complicated analytical fits in favor of more accurate interpolation schemes. In the present computation we have used the weighted Shepard interpolation scheme as implemented by Renka.[47]

Ther IR absorption spectrum from the initial state Ψ_i to the final state Ψ_f is given approximately as[48]

$$I_\mathrm{i}(\omega) = \sum_{\alpha=x,y,z} \sum_f \omega_{\mathrm{fi}} |\int \mathrm{d}\mathbf{q} \Psi_f(\mathbf{q})\, d^\alpha(\mathbf{q}) \Psi_\mathrm{i}(\mathbf{q})|^2\, \delta(\omega - \omega_{\mathrm{fi}}) \quad (6)$$

where $\omega = \omega_{\mathrm{fi}}$ is the transition frequency and $d^\alpha(\mathbf{q})$ are the Cartesian components of the dipole moment operator. The system is in the $x-y$ plane, and the z-axis is perpendicular. Obviously, there is no contribution in the z-direction as we did not include any out-of-plane modes.

An attractive feature of the normal mode approach is the assignment in terms of uncoupled normal modes,[14,42] so-called zero order states, given by

$$H_0 = \sum_i \left[\frac{P_i^2}{2\mu_i} + V(q_i, \{q_{j\neq i} = 0\}) \right] \quad (7)$$

The contribution of a particular eigenstate $\Psi_k^{(0)}$ of H_0 to the eigenstate of the full Hamiltonian

$$H = \sum_i \left[\frac{P_i^2}{2\mu_i} + V(\mathbf{q}) \right] \quad (8)$$

is given by the coefficients C_{lk}

$$\Psi_l = \sum_k C_{lk} \Psi_k^0 \quad (9)$$

III.2 Internal Coordinate Representation. An exact full-dimensional quantum treatment of the proton tunneling dynamics in ACAC is not feasible. We resort, therefore, to an approximate reduced dimesionality computation in internal, large amplitude coordinates. The three symmetry adapted coordinates

we shall use are

$$q_1 = r_1 + r_2$$
$$q_2 = r_2 - r_2 \qquad (10)$$
$$q_3 = \theta$$

where r_1 is the distance from the hydrogen to the donor oxygen atom, r_2 is the distance from the hydrogen to the acceptor oxygen atom, and θ is the OHO angle. These coordinates are designed to capture some basic features of the proton-transfer moiety of ACAC: q_1 and q_2 describe the symmetric and asymmetric proton motion, while q_3 accounts for the distance between the two oxygen atoms. Among others, a related set of coordinates has been used by Shida and Almof for treating the proton tunneling in MA[5] by the reaction surface Hamiltonian approach, and recently by Špirko et al.[49] in a study of the dimensionality of the proton-transfer reaction in formimidol. The large barrier height for *syn-anti* isomerization of 16.2 kcal mol^{-1} at the B1LYP/6-311G(d,p) level of theory, and the lower barrier to proton transfer in ACAC compared to MA, indicates that the in-plane motion of the bridging proton is strongly favored. Consequently, in the PES calculations the planarity of the chelate ring was assumed, and the methyl groups were fixed in the eclipsed conformation which enhances proton tunneling. All other degrees of freedom were optimized. In fact, the full optimization of the PES was attempted, but, because of the extreme floppiness of the methyl groups, the calculation turned out to be numerically prohibitive. The potential and dipole surfaces were calculated on a variable grid in the q_1 and q_2 direction. For $q_3 = 107°$ the $q_1 \times q_2$ grid size was 15×16, while for $q_3 = 187°$ the size was 10×10.

The coupling of the 3D subspace of internal degrees of freedom to other degrees of freedom of the molecules can approximatively be taken into account through the coordinate dependence of the Wilson *G*-matrix elements. Following Alexandrov et al.,[38,50] we found that it was advantageous to first evaluate the matrix elements of the G_{rs} matrix

$$G_{rs} = \sum_{i=1}^{3N} m_i \frac{\partial x_i}{\partial q_r} \frac{\partial x_i}{\partial q_s} \qquad (11)$$

and then invert the 3×3 G_{rs} matrices to obtain G^{rs}.

Specifically for fixed values of two chosen internal coordinates, the atomic Cartesian coordinates x_i were 1D spline-interpolated along the third coordinate. The same procedure was repeated for all three internal coordinates. As there are 45 Cartesian coordinates in ACAC, more than 15000 1D − spline interpolated functions were required in order to evaluate $\partial x_i/\partial q_r$ and $\partial x_i/\partial q_s$ at each point of the grid. To avoid spurious effects in the derivatives it is important that all structures resulting from the displacements δq_r conform to the Eckart conditions.[51] Here the reference geometry to which each conformation was rotated and translated was the C_{2v} structure of the transition state for the proton-transfer reaction (**TS1**).

The 3D potential and dipole surfaces and the six symmetry-unique G^{rs}, $r = 1, 3$; $s = 1, 3$ surfaces were interpolated to a $25 \times 25 \times 25$ direct product grid in the range (Angstroms) of $2.15 \le q_1 \le 4.05$, $-2.0 \le q_2 \le 2.0$, and $107° \le q_3 \le 187°$. The Schrödinger equation

$$[\hat{T}_q + V(q_1, q_2, q_3)]\Psi_{l,m,n}(q_1, q_2, q_3) = E_{l,m,n}\Psi_{l,m,n}(q_1, q_2, q_3) \qquad (12)$$

with the kinetic energy opperator $\hat{T}_q$ given in eqs 1, 3, and 4 is then solved. Eigenvalues and eigenfunctions of the vibrational Hamiltonians were obtained using the Fourier grid Hamiltonian method in internal coordinates.[38] As in the previous section for the diagonalization, we have used the implicitly restarted Lanczos method[44] implemented in the ARPACK package.[45,46]

The tunneling splitting of the ground-state i.e., the vibrational transition frequency from the symmetric, 0(+), to the asymmetric, 0(−), ground state is simply the difference between the two lowest eigenvalues:

$$\omega(0(+) \rightarrow 0(-)) = E_{100} - E_{000} \qquad (13)$$

By analogy the vibrational transition frequencies of the O−O stretching doublet are $\omega(0(+) \rightarrow 1(-)) = E_{101} - E_{000}$ and $\omega(0(-) \rightarrow 1(+)) = E_{001} - E_{100}$. Since the relationship between the OH-stretching mode and the selected internal coordinates is not easy, our assignments are based on the comparison between IR intensities, $I_0(\omega)$, obtained from the d^x and d^y components of the dipole moment separately (see eq 6 and section IV).

The 3D PES revealed characteristic features for large amplitude proton motion in double well potentials: at short interoxygen separations the bridging proton experiences a single well PES, while by increasing the interoxygen distance, the barrier to proton transfer rises and proton tunneling sets in.

The strength of the coupling between the vibrations of the O−H···O moiety and the remaining modes of the ACAC **TS2** conformer is of high importance for assessing the accuracy of the approximate vibrational kinetic energy operators given in eqs 3−4. The coordinate dependence of the *G*-matrix elements shown in Figure 4 provides information about these couplings. The presented results are, actually, 2D projections of the *G*-matrix for the shortest interoxygen separation of $q_3 = 187°$. All *G*-matrix elements display a considerable coordinate dependence, with the G^{22} term varying between 1.7 and 4.3 amu. For the particular choice of internal coordinates given in eq 10 the coupling terms $-0.08 \le G^{12} \ge 0.08$, $-0.07 \le G^{13} \ge 0$, and $-0.4 \le G^{23} \ge 0.04$ are small when compared to the diagonal ones. Consequently, one expects eq 3 to give a more accurate description of the H-bond dynamics than eq 4.

IV. Results and Discussion

IV.1 Normal Mode Representation. Figure 5 shows the computed vibrational spectra of the ACAC **SYN** (upper panel) and **TS2** (lower panel) conformers. A temperature of 297 K was assumed. Transitions from the ground state (I_0) are shown in black, while hot transitions, i.e., these starting from the vibrationally excited $\nu_{OH\cdots O}$ and $\nu_{O\cdots O}$ modes are shown by dashed lines. In Figure 6 we display the experimental gas-phase IR spectrum[23] in comparison with the summed up spectrum of the two species. For the low-frequency part of the experimental spectrum we refer to the 1966 article of Ogoshi et al.[17] Further, Table 3 compiles the calculated fundamental transitions and the coefficients for the decomposition of these transitions in terms of zero-order states (see eq 9).

At first glance, the lines at 227 and 363 cm^{-1} correspond to the $\nu^{SYN}_{OH\cdots O}$ and $\nu^{SYN}_{O\cdots O}$ modes. Both fundamentals are in very good agreement with the observed in-plane ring deformation modes at 230 and 364 cm^{-1}. The calculated $\nu^{TS2}_{O\cdots O}$ frequency is 349 cm^{-1}, but compared to $\nu^{SYN}_{O\cdots O}$ it has a negligible intensity.

The in-plane bending fundamental transition δ^{SYN}_{OH} is at 1375 cm^{-1}. Compared to the harmonic frequency of 1402 cm^{-1} it is red-shifted by only 27 cm^{-1}. This harmonic nature of the

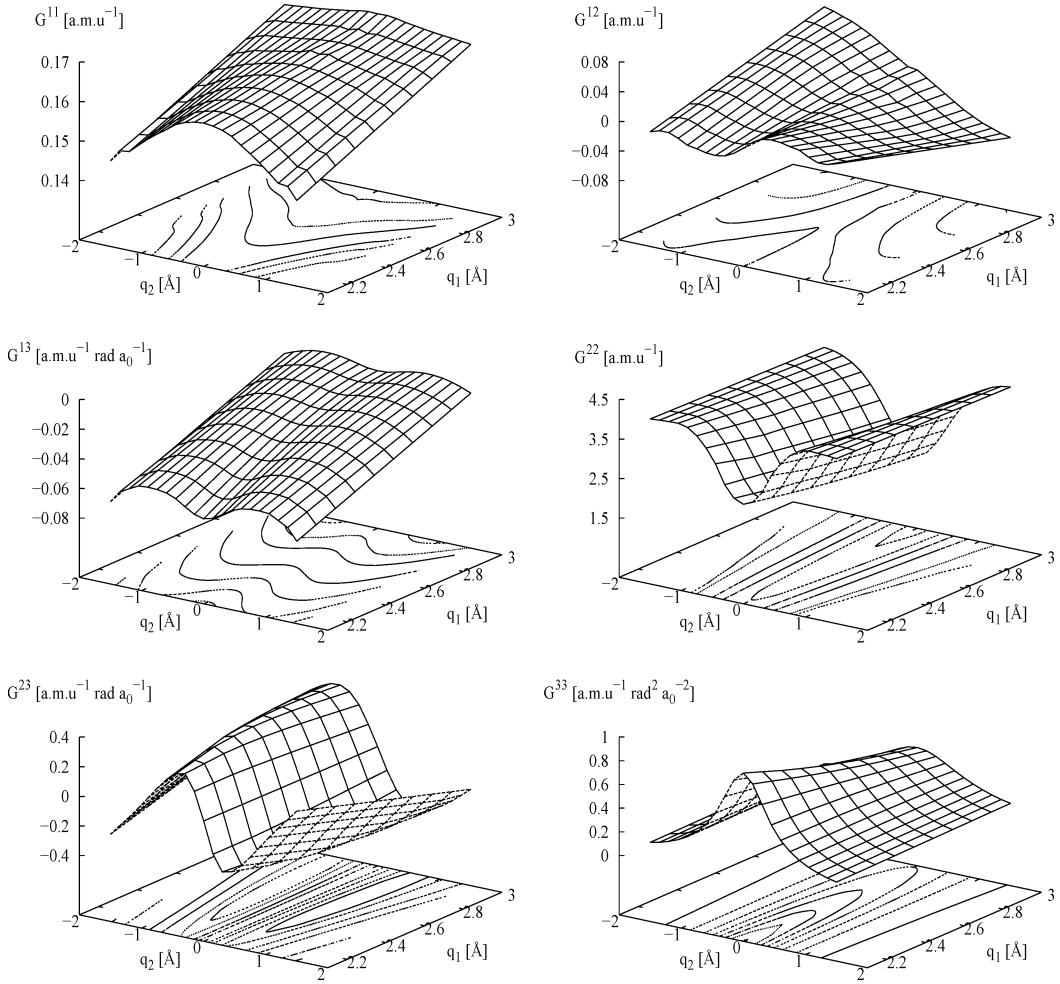

Figure 4. 2D projections of the *G*-matrix elements at $q_3 = 187°$ for the **SYN** ACAC.

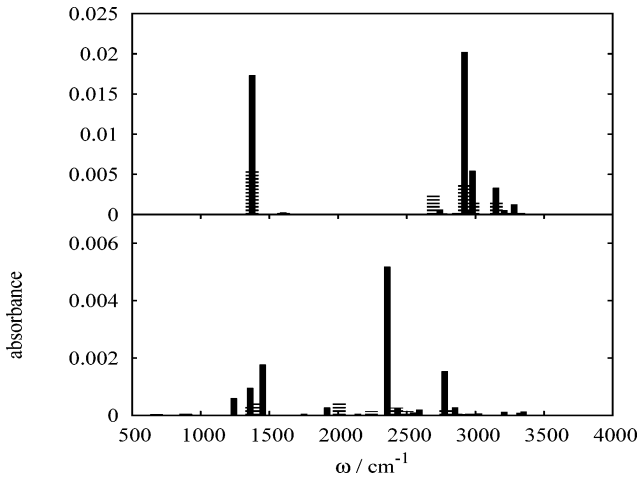

Figure 5. IR stick spectra of ACAC **SYN** (upper panel) and **TS2** (lower panel) conformers at $T = 297$ K. Transitions from the ground state are shown in black, hot transitions from $\nu_{OH\cdots O}$ and $\nu_{O\cdots O}$ are shown in gray.

bending fundamental can be inferred from Table 3 where the dominant coefficient comes from the transition to the (0,1,0,0) state, with a minor contribution of the (0,1,0,1) state. The situation is rather different with the δ_{OH}^{TS2} transition at 1360 cm^{-1}. As can be seen, the transition gains in intensity and develops a double-maxima structure due to a resonance with the $\nu_{O\cdots O}^{TS}$ overtone. The remaining $\approx$50 cm^{-1} discrepancy between the calculated and observed δ_{OH} is puzzling, as it cannot be attributed to the couplings triggered by the hydrogen bond formation. The δ_{OH}^{TS2} anharmonic frequency of 1318 cm^{-1} (see Table 2) is in good agreement with experiment but does not reveal the source of anharmonicity. We, therefore, performed a pairwise analysis of the part of the PES spanned by the bending coordinate and found that the red-shift of the mode is due to mixing with two other modes containing OH-bending contributions: the ν_9 (OH-bend/asymmetric C═C−C═O stretch) and the ν_{10} (OH-bend/symmetric C═O stretch). Consequently, the transition at 1298 cm^{-1} [52] is assigned to the δ_{OH}^{TS2} mode and a previously unassigned transition at $\approx$1360 to δ_{OH}^{SYN} (see the deconvoluted IR spectrum in Tayyari et al.[21]).

IV.1.1 The OH-Stretching Region. In the following we focus on the OH-stretching region, undoubtedly the most intriguing part of the infrared spectrum. According to Table 3 the most relevant transitions in the ν_{OH}^{SYN} stretching region, between 2900 and 3500 cm^{-1}, decompose into *all* zero-order states. Therefore, it is not possible to identify any transition of the ν_{OH} band as a ν_{OH}^{SYN} fundamental. The fact that the ν_{OH}^{SYN} fundamental is distributed in several states of the OH-stretch band leads to the well-known difficulties in assignments of the OH-stretch band. This, in its turn, is an important consequence of the strong anharmonic mode mixing triggered by the H-bond formation. A further consequence is the breakdown of the vibrational selection rule which implies a change of the vibrational quantum numbers by one. For example, the hot transition of the in-plane bending mode (0,0,0,1) → (0,1,0,1) occurs at the same frequency as the fundamental (0,0,0,0) →

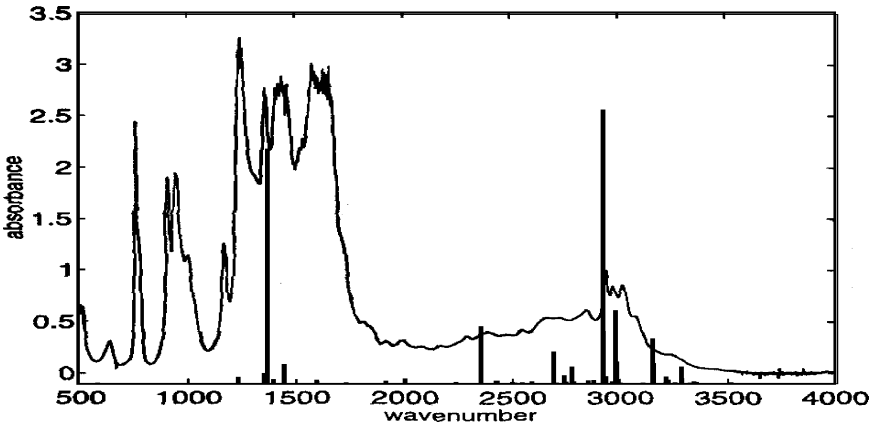

Figure 6. The computed IR spectrum of both conformers at $T = 297$ K superimposed on the experimental gas-phase spectrum (courtesy of J. Mavri and J. Grdadolnik).[23] The computed intensities have been rescaled in order to facilitate comparison with experiment.

TABLE 3: Coefficients of the Zero Order States (eq 9) of Those States Corresponding to the Strongest Transitions in the OH-stretch Bands of the SYN and TS2 ACAC[a]

SYN							TS2					
f	ω/cm^{-1}	N_{q1}	N_{q2}	N_{q3}	N_{q4}	c_{if}	f	ω/cm^{-1}	N_{q1}	N_{q2}	N_{q3}	c_{if}
1	228	0	0	0	1	0.947	1	349	0	0	1	−0.867
2	364	0	0	1	0	0.959	4	1240	0	1	0	0.632
16	1375	0	1	0	0	−0.958			0	0	3	0.328
		0	1	0	1	0.213			0	1	1	0.292
63	2742	0	1	0	0	−0.914	5	1360	0	1	0	−0.433
		0	2	0	1	0.260			0	0	3	0.559
70	2920	1	0	0	0	0.614			0	0	4	0.399
		1	0	0	1	−0.412			0	0	5	0.299
		1	0	0	2	0.216	6	1451	0	1	0	−0.549
		0	2	0	0	0.275			0	0	4	−0.453
		0	2	0	1	0.275			0	0	5	−0.262
		1	0	1	0	−0.249	9	1290	0	0	5	0.403
74	2977	0	2	0	0	−0.207			0	1	2	−0.314
		0	2	0	1	−0.792			0	1	3	−0.252
		0	2	0	2	0.304	12	2357	1	0	0	0.539
		1	0	0	0	0.356			1	0	1	0.418
83	3149	1	0	0	0	−0.431			1	0	2	0.230
		1	0	0	1	−0.355	16	2776	0	2	0	0.680
		1	0	0	2	0.419			0	2	1	0.290
		1	0	0	3	−0.252						
		0	2	0	1	−0.216						
		0	2	0	2	−0.253						
89	3210	0	2	0	1	−0.300						
		0	2	0	2	−0.720						
		0	2	0	3	0.294						
		1	0	0	0	0.205						
		1	0	0	1	0.289						
		1	0	0	2	−0.212						
91	3281	0	2	1	0	−0.241						
		0	2	1	1	−0.251						
		1	0	0	0	−0.321						
		1	0	1	0	−0.485						
		1	0	1	1	0.344						
		1	0	2	0	0.307						
		1	0	2	1	−0.206						

[a] The results are obtained in the normal mode representation.

(0,1,0,0) transition, but in the ν_{OH} region the transitions starting from (0,0,0,1) (gray bars) are shifted by the amount of the initial excitation.

The OH-stretch band is dominated by a closely spaced doublet at 2920 and 2977 cm^{-1} with resonance enhanced intensities. As expected, the underlying dynamics is more complex than what a Fermi resonance phenomenon would suggest. In addition to the excitation of the OH-bending and OH-stretching modes, the transitions at 2977 cm^{-1} contain noticeable excitation of the low-frequency modes. The same is valid for the Franck−Condon type vibrational progression observed within the ν_{OH}^{SYN} band. Although the energy differences between the states $f = 70$ and $f = 83$, and between $f = 70$ and $f = 91$ (see Table 3) match exactly the frequencies of the $\nu_{OH\cdots O}^{SYN}$ and $\nu_{O\cdots O}^{SYN}$ modes, respectively, the analysis reveals zero order states of similar magnitude. Consequently, an interpretation in terms of combination transitions such as $\delta_{OH} + N\delta_{O\cdots O} + M\delta_{OH\cdots O}$ is an oversimplified view of O−H···O fragment dynamics.

Let us now turn attention to the comparison with the observed IR spectrum (Figure 6). Although the two maxima coincide within few wavenumbers, and the local maxima structure is also well reproduced, important differences lie in the intensities and

TABLE 4: Vibrational Transition Frequencies and Intensities for the TS2 Ground State Doublet from the Fully Coupled Calculation (eq 1) and Two Approximate Calculations (eq 3 and eq 4)

	eq 1		eq 3		eq 4	
	freq/cm^{-1}	Int.	freq/cm^{-1}	Int.	freq/cm^{-1}	Int.
ground state						
O(+) → O(−)	116	0.1321	89	0.1480	208	0.1058
O−O mode						
O(+) → 1(−)	523	0.00075	555	0.00013	632	0.00366
O(−) → 1(+)	224	0.0339	284	0.0308	191	0.0332
O−H stretching						
O(+) → 1(−)	2683	0.0030	2539	0.0032	2816	0.0020
O(−) → 1(+)	1830	0.0041	1734	0.0027	1706	0.0020

in the width of the bands. Note that our IR intensities have been rescaled in order to facilitate comparison with the experiment.[23] While the IR spectrum of ACAC displays a very broad ν_{OH} band in the 1800−3400 cm^{-1} region, the computed spectrum does not contain transitions of noticeable intensity below 2650 cm^{-1}. An extension of the model 4D system, for example by including the symmetric and asymmetric C═O stretch motion, will increase the number of transitions and, to a certain extent, will modify the band shape. However, examination of the energies of the C═O fundamentals given in Table 2 indicates that changes are expected on the high-frequency side of the band, i.e., in the region where the Fermi resonance condition is fulfilled.

To elucidate the causes of the OH-stretch band broadening, we consider the spectrum of the **TS2** conformer. The strongest transition in the ν_{OH}^{TS2} band is located at 2357 cm^{-1}. Compared to the corresponding **SYN** transition, it is red-shifted by more than 500 cm^{-1}. The transition is also red-shifted by about 130 cm^{-1} with respect to its anharmonic value given in Table 2. These observations lead to the conclusion that both *enol*-ACAC conformers, **SYN** and **TS2**, contribute to the formation of the OH-stretching band. Due to the particular choice of normal modes spanning the 3D PES, there is no evidence for Fermi resonance interactions in the band. Namely, for consistency reasons, the 4D and 3D PESs of the **SYN** and **TS2** conformers were spanned by an analogous set of modes, but in **TS2** the frequency difference between δ_{OH}^{TS2} and ν_{OH}^{TS2} prevents a resonance interaction. Instead, inspection of Table 2 reveals a possible Fermi resonance condition occurring with ν_{19} (OH-bend/symmetric C═C stretch) at 1240 cm^{-1}, which will contribute to build up intensity around 2500 cm^{-1}.

The spectrum shown in Figure 6 represents our best result achieved under the single-well, normal-mode approximation. While the overall agreement with experiment appears to be quite satisfactory, consistency requires the inclusion of the proton tunneling motion. In principle, the double well proton motion should leave a mark in the IR spectrum of ACAC and, according to our reaction path calculations,[33] evidence of proton tunneling is most likely to show up in the spectrum of **TS2**.

IV.2 Tunneling. In Table 4 we give the vibrational energy levels of the ground and excited states of ACAC as obtained by employing eqs 1, 3, and 4. The rigorous, i.e., fully coupled, Hamiltonian predicts a ground-state splitting of 116 cm^{-1}. By neglecting the mixed derivative terms one obtains a tunneling splitting of 88 cm^{-1}. Apparently, the symmetric vibrational coordinates given in eq 10 contain the error that arises from decoupling of eq 1. A rather different situation is encountered in the constant *G*-matrix case where a tunneling splitting of 207 cm^{-1} is obtained. These results confirm our suspicion of the inadequacy of eq 4 to describe large amplitude proton motion. The proton-transfer process is, clearly, a collective molecular motion and the accompanying geometrical changes have to be accounted for both in the potential and in the kinetic energy operators.

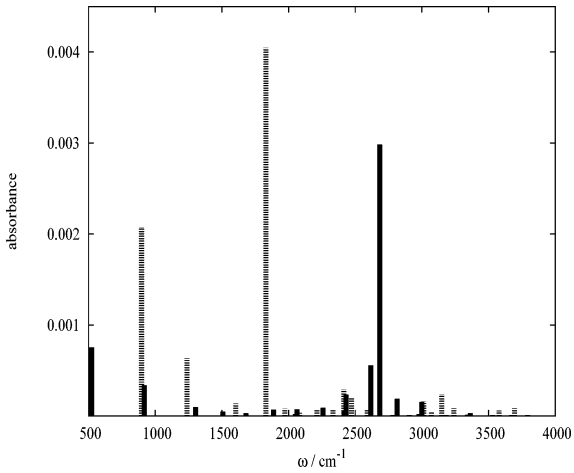

Figure 7. IR stick spectrum of the ACAC **TS2** conformer at $T = 297$ K in the 500−4000 cm^{-1} region obtained in the internal coordinate representation. Transitions from the symmetric (solid black bars) and asymmetric (open dashed bars) ground states are shown on the same plot.

In contrast to the normal mode description, where the line assignments in terms of zero-order states were straightforward, here the assignments, based on inspection of the wave functions plots, are more difficult. Valuable additional insight into the nature of the transitions is obtained by considering separately the contributions from the d^x and d^y vector components of the dipole moment. As we are interested in the excitation of the stretching transitions, the focus is on the d^x component of the dipole moment. For the O−O stretching doublet (ring deformation) the calculation yields 224 and 523 cm^{-1}. The two transitions find correspondence in the observed $\nu_{OH\cdots O}$ mode and to the ν_{33} ring deformation mode assigned at 508 cm^{-1}.

The calculated stick IR spectrum in the frequency range 500−4000 cm^{-1} is displayed in Figure 7. The transitions from the symmetric 0(+) ground state are shown in black and these from the asymmetric, 0(−), state are in gray. The calculated peaks at 2683 and (1830) cm^{-1} are assigned to transitions from the symmetric (asymmetric) ground state to vibration with asymmetric (symmetric) OH-stretch character. Thus, in the fully coupled case a tunneling induced splitting of 853 cm^{-1} is obtained, whereas the uncoupled Hamiltonian (eq 3) yields 806 cm^{-1}. Here again the constant *G*-matrix approximation overestimates the splittings, yielding more than 1100 cm^{-1}. Due to the strong promoting character of the OH-stretching mode, such large tunneling splitting was expected. Comparison with the normal mode calculations shows a blue shift of the 0(+) → OH, 1(−) transition by about 300 cm^{-1} and a red shift of the 0(−) → OH, 1(+) transitions by more than 500 cm^{-1}. The

results are given with respect to the TS2 most intense transition at 2357 cm^{-1}. Now, we remind the reader that the calculations were performed under the assumption of the planarity of the molecular ring. It is, therefore, reasonable to expect that the energy levels of the excited vibrational states are overestimated. Based on experience with malonaldehyde,[8] on a nonplanar PES the value for the OH-stretch vibrational energy levels would be lower by about 100−200 cm^{-1}. Note, however, that a much smaller error is expected for the splittings.

Compared to the experimental IR spectrum, the computed 0(+) → OH,1(−) and 0(−) → OH,1(+) frequencies lie within the OH-stretch band. The peak at 1730 cm^{-1} visible in the IR spectrum of Figure 6 belongs to the ACAC keto tautomer. However, in the broad C═O stretch region, an interesting, three maxima peak structure is reported. Cohen and Weiss[31] found that the intensity of the middle component at 1630 cm^{-1} increases with temperature, whereas in the spectra of the deuterated compound (d2-ACAC) only two components are observed at all temperatures. Although they found indications of proton tunneling, on the basis of a 1D double well model calculation,[53] the authors disregarded the possibility that the temperature dependent transition is actually a manifestation of the proton tunneling motion. Instead, they assumed that the structure of the C═O band is due to the coexistence of two forms of the *enol*-ACAC: the ground state and a low-lying vibrationally excited state. On the other hand, on the basis of a harmonic normal-mode analysis, Tayyari et al.[21] assigned the transitions to the **SYN** and **TS2** forms of ACAC. The anharmonic frequencies given in Table 2 show that the **SYN** modes ν_9 (ν_a C═C−C═O + δ OH) at 1650 cm^{-1} and ν_{10} (ν C═O + δ OH) at 1625 cm^{-1} shift in **TS2** for only few wavenumbers to 1644 and 1628 cm^{-1}, respectively. Consequently, the three maxima structure of the C═O band cannot be easily explained by the coexistence of the **SYN** and **TS2** forms of ACAC. All of the above point to the possibility of an alternative assignment. The three-peak structure could be the manifestation of the ground level splitting in the **TS2** C═O bands,[54] but then the temperature dependence of only one peak is disturbing. We are, therefore, tempted to assign the peak at 1630 cm^{-1} to the 0(−) → OH,1(+) transition. Due to the ground-state tunneling splitting of 116 cm^{-1}, the intensity of the 0(−) → OH,1(+) transition ought to be temperature dependent, supporting the assignment. For a more definitive assignment, however, an extension of the dimensionality of the model and the full optimization of the PES are required.

V. Conclusion

We have conducted reduced-dimensional quantum studies of the vibrational energy levels of acethylacetone. To analyze the shared proton vibrations we employed two sets of coordinates: normal mode coordinates describing the PES in vicinity of the most stable configuration, and internal coordinates accounting for the double minimum proton motion.

(i) Within the normal mode approach we were capable of proving that the extremely broadened OH-stretch band in ACAC is a consequence of the coexistence of two *enol*-ACAC forms: the global minimum structure **SYN** and the transition state for the rotation of the distal methyl group **TS2**. The evidence for this comes from the fact that in the spectra of the two conformers the most intense transitions involving ν_{OH} excitations are separated by more than 500 cm^{-1}. Since the ν_{OH} fundamental is distributed into all modes of the O−H···O fragment subspace, and Franck−Condon-like vibrational progressions contribute to broadening of the OH-stretch band, it is not possible to distinguish the two bands in the experimental IR spectrum. However, the low interconversion barrier between the two forms points to a temperature dependence of the OH-stretch band that is in agreement with NMR studies of the chemical shift of the enolic proton. While the above issue is specific for ACAC, we have good reason to believe that patterns that emerged in our study, such as: disappearance of the ν_{OH} fundamental and strong mixing of the low-frequency modes of the molecular framework, represent general features of the vibrational dynamics of intramolecular H-bonds. These findings are in accord with the model studies of the Perpignan group,[27,29] but the uncovered dynamics is, distinctly, more complex.

(ii) The study of the proton transfer motion by means of fully coupled large amplitude coordinates led to the evaluation of the **TS2** ground-state tunneling splitting of 116 cm^{-1}. In the OH-stretch direction a splitting of 853 cm^{-1} was predicted. According to our calculation, the possibility that the three-component structure of the C═O stretch band is actually due to the double-well proton motion, i.e., to the 0(−) → OH,1(+) transition, cannot be ruled out.

In parallel we have investigated the strength of the coupling among vibrations of the O−H···O fragment, as well as the coupling to vibrations lying outside the fragment subspace. In the symmetry adapted set of coordinates we have used, the system is nearly separable. However, the multidimensional nature of the shared proton vibration is reflected in the strong coordinate dependence of the elements of the Wilson *G* matrix. In this respect, we want to emphasize the importance of including accurate kinematic coupling when treating intramolecular proton-transfer systems in reduced-dimensionality.

Acknowledgment. This work has been supported by the Croatian Ministry of Science and Technology under Project 0098033. N.D. is grateful to B. R. Johnson, V. Mohacek-Grosev, and J. Stare for stimulating discussions.

References and Notes

(1) Rowe, W. F.; Duerst, R. W.; Wilson, E. B. *J. Am. Chem. Soc.* **1976**, *98*, 4021.
(2) Baughcum, S. L.; Duerst, R. W.; Rowe, W. F.; Smith, Z.; Wilson, E. B. *J. Am. Chem. Soc.* **1981**, *103*, 6296.
(3) Baba, T.; Tanaka, T.; Morino, I.; Yamada, K. M. T.; Tanaka, K. *J. Chem. Phys.* **1999**, *110*, 4131.
(4) Carrington, T.; Miller, W. H. *J. Chem. Phys.* **1986**, *84*, 4364.
(5) Shida, N.; Barbara, P. F.; Almlöf, J. E. *J. Chem. Phys.* **1989**, *91*, 4061.
(6) Benderskii, V. A.; Vetoshkin, E. V.; Irgibaeva, I. S.; Trommsdorff, H. P. *Chem. Phys.* **2000**, *262*, 393.
(7) Yagi, K.; Taketsugu, T.; Hirao, K. *J. Chem. Phys.* **2001**, *115*, 10647.
(8) Babić, D.; Bosanac, S. D.; Došlić, N. *Chem. Phys. Lett.* **2002**, *358*, 337.
(9) Mil'nikov, G. V.; Yagi, K.; Nakamura, H.; Taketsugu, T.; Hirao, K. *J. Chem. Phys.* **2003**, *119*, 10.
(10) Meyer, R.; Ha, T.-K. *Mol. Phys.* **2003**, *101*, 3263.
(11) Mil'nikov, G. V.; Yagi, K.; Nakamura, H.; Taketsugu, T.; Hirao, K. *J. Chem. Phys.* **2004**, *120*, 5036.
(12) Coutinho-Neto, M. D.; Viel, A.; Manthe, U. *J. Chem. Phys.* **2004**, *121*, 9207.
(13) Hayashi, T.; Mukamel, S. *J. Phys. Chem.* **2003**, *107*, 9113.
(14) Došlić, N.; Kühn, O. *Z. Phys. Chem.* **2003**, *217*, 1507.
(15) Khalil, M.; Demirdoven, N.; Tokmakoff, A. *J. Phys. Chem. A* **2003**, *107*, 5258.
(16) Smith, Z.; Wilson, E. B.; Duerst, R. W. *Spectrochim. Acta A* **1983**, *39*, 1117.
(17) Ogoshi, H.; Nakamoto, K. *J. Chem. Phys.* **1966**, *45*, 3113.
(18) Folkendt, M. M.; Weiss-Lopez, B. E.; Chauvrel, J. P.; True, N. S. *J. Phys. Chem.* **1985**, *89*, 3347.
(19) Johnson, M. R.; Jones, N. H.; Geis, A.; Horsewill, A. J.; Trommsdorff, H. P. *J. Chem. Phys.* **2002**, *116*, 5694.
(20) Dannenberg, J. J.; Rios, R. *J. Phys. Chem.* **1994**, *98*, 6714.
(21) Tayyari, S. F.; Milani-nejad, F. *Spectrochim. Acta A* **2000**, *56*, 2679.
(22) Mavri, J.; Grdadolnik, J. *J. Phys. Chem.* **2001**, *105*, 2039.

(23) Mavri, J.; Grdadolnik, J. *J. Phys. Chem.* **2001**, *105*, 2045.
(24) Sliznev, V. V.; Lapshina, S. B.; Girichev, G. V. *J. Struct. Chem.* **2002**, *43*, 47.
(25) Heyne, K.; Huse, N.; Nibbering, E. T. J.; Elsaesser, T.; Mukamel, S. *J. Chem. Phys.* **2004**, *121*, 902.
(26) Watson, J K. G. *Mol. Phys.* **1968**, *15*, 479.
(27) Belharaya, K.; Blaise, P.; Henri-Rousseau, O. *Chem. Phys.* **2003**, *293*, 9.
(28) Kühn, O. *J. Phys. Chem.* **2002**, *106*, 7671
(29) Belharaya, K.; Chamma, D.; Henri-Rousseau, O. *Chem. Phys.* **2003**, *293*, 31.
(30) Tayyari, S. F.; Zeegers-Huyskens, Th.; Wood, J. L. *Spectrochim. Acta A* **1979**, *35*, 1289.
(31) Cohen, B.; Weiss, S. *J. Phys. Chem.* **1984**, *88*, 3159.
(32) Horsewill, A. J.; Alsanoosi, A. M.; Carlisle, C. J. *J. Phys. C* **1987**, *20*, L869.
(33) Matanović, I.; Došlić, N.; Mihalić, Z. *Chem. Phys.* **2004**, *306*, 201.
(34) Adamo, C.; Barone, V. *Chem. Phys. Lett.* **1997**, *274*, 242
(35) Frisch, M. J.; Trucks, G. W.; Schlegel, H. B.; Scuseria, G. E.; Robb, M. A.; Cheeseman, J. R.; Montgomery, J. A., Jr.; Vreven, T.; Kudin, K. N.; Burant, J. C.; Millam, J. M.; Iyengar, S. S.; Tomasi, J.; Barone, V.; Mennucci, B.; Cossi, M.; Scalmani, G.; Rega, N.; Petersson, G. A.; Nakatsuji, H.; Hada, M.; Ehara, M.; Toyota, K.; Fukuda, R.; Hasegawa, J.; Ishida, M.; Nakajima, T.; Honda, Y.; Kitao, O.; Nakai, H.; Klene, M.; Li, X.; Knox, J. E.; Hratchian, H. P.; Cross, J. B.; Adamo, C.; Jaramillo, J.; Gomperts, R.; Stratmann, R. E.; Yazyev, O.; Austin, A. J.; Cammi, R.; Pomelli, C.; Ochterski, J. W.; Ayala, P. Y.; Morokuma, K.; Voth, G. A.; Salvador, P.; Dannenberg, J. J.; Zakrzewski, V. G.; Dapprich, S.; Daniels, A. D.; Strain, M. C.; Farkas, O.; Malick, D. K.; Rabuck, A. D.; Raghavachari, K.; Foresman, J. B.; Ortiz, J. V.; Cui, Q.; Baboul, A. G.; Clifford, S.; Cioslowski, J.; Stefanov, B. B.; Liu, G.; Liashenko, A.; Piskorz, P.; Komaromi, I.; Martin, R. L.; Fox, D. J.; Keith, T.; Al-Laham, M. A.; Peng, C. Y.; Nanayakkara, A.; Challacombe, M.; Gill, P. M. W.; Johnson, B.; Chen, W.; Wong, M. W.; Gonzalez, C.; Pople, J. A. *Gaussian 03*, revision B.05; Gaussian, Inc.: Pittsburgh, PA, 2003.
(36) Barone V.; Manichino, C. *J. Mol. Struct.* **1995**, *330*, 365.
(37) Califano S. *Vibrational States*; John Wiley & Sons: Ltd.: London, 1996.
(38) Stare J.; Balint-Kurti, G. G. *J. Phys. Chem.* **2003**, *107*, 7204.
(39) Alparone, A.; Millefiori S. *Chem. Phys.* **2003**, *290*, 15.
(40) Tew, D. P.; Handy, N. C.; Carter, S.; Irle, S.; Bowman J. *Mol. Phys.* **2003**, *101*, 3513.
(41) Dai J.; Bačić, Z.; Huang, X.; Carter, S.; Bowman, J. M. *J. Chem. Phys.* **2003**, *119*, 6571.
(42) Beil, A.; Hollenstein, H.; Monti, O. L. A.; Quack, M.; Stohner, J. *J. Chem. Phys.* **2000**, *113*, 2701.
(43) Marston, C. C.; Balint-Kurti, G. *J. Chem. Phys.* **1989**, *91*, 3571.
(44) Golub, G. H.; Van Loan, C. F. *Matrix Computations*; The Johns Hopkins University Press: Baltimore, 1985.
(45) Sorensen, D. *Tutorial: Implicitly Restarted Arnoldi/Lanczos Methods for Large Scale Eigenvalue Calculations*; Rice University: Houston, 1995.
(46) Lehoucq, R. B.; Sorensen, D.; Yang, C. *ARPACK User's Guide: Solution of Large Scale Eigenvalue Problems with Implicitly Restarted Arnoldi Methods*; Rice University: Houston, 1997.
(47) Renka, R. J. *ACM Trans. Math. Software* **1988**, *14*, 151.
(48) May, V.; Kühn, O. *Charge and Energy Transfer Dynamics in Molecular Systems*; Wiley-VCH: Berlin, 2000.
(49) Špirko, V.; Čejchan, A.; Lutchyn, R.; Leszczynski, J. *Chem. Phys. Lett.* **2002**, *355*, 319.
(50) Alexandrov, V.; Smith, D. M. A.; Rostkowska, H.; Nowak, M. J.; Adamowicz, L.; McCarthy, W. *J. Chem. Phys.* **1998**, *108*, 9685.
(51) Wilson, E. B.; Decius, J. C.; Cross, P. C. *Molecular Vibrations*; Dover Publications: New York, 1995.
(52) Chiavassa, T.; Verlaque, P.; Pizzala, L.; Roubin, P. *Spectrochim. Acta A* **1994**, *50*, 343.
(53) Somorjai, R. L.; Hornig, D. F. *J. Chem. Phys.* **1962**, *36*, 1980.
(54) Duan, C. X.; Luckhaus, D. *Chem. Phys. Lett.* **2004**, *391*, 129.